RSC Advances

PAPER

View Article Online
View Journal | View Issue

Cite this: *RSC Adv.*, 2022, **12**, 34393

Activated carbon from almond shells using an eco-compatible method: screening, optimization, characterization, and adsorption performance testing

H. Boulika, *[a] M. El Hajam,[ab] M. Hajji Nabih,[a] N. Idrissi Kandri[a] and A. Zerouale[b]

Activated carbon as a low-cost adsorbent prepared from almond shells using H_3PO_4 as a chemical activator and room vacuum pyrolysis as a physical activator, which is considered to be an eco-compatible preparation process. Experimental design methodology was used to study and optimize the effects of eight preparation parameters on I_2 adsorption expressed by the iodine index (mg g^{-1}). It was found that optimum activated carbon was obtained by chemical activation with H_3PO_4 at first, followed by physical treatment at 420 °C under a vacuum pressure of −0.8 bar. The obtained activated carbon was characterized by a thermogravimetric analyzer, scanning electron microscopy coupled to EDX, X-ray diffraction, and Fourier transform infrared absorption spectroscopy. The zero-charge pH and the characteristics of surface chemistry by Boehm titration were determined to predict the acid–base properties of the prepared material. An adsorption efficiency study of crystal violet dye on the optimally produced activated carbon was carried out. The obtained results of physicochemical characterization showed interesting properties of our activated carbon in comparison with those produced by other methods. Among these properties, an important porous surface, high thermal stability, and a disorganized graphitic crystalline structure were revealed. In addition to the carbon and oxygen elements, EDX analysis revealed the presence of phosphorus element, and the FTIR analysis indicated the existence of phosphonate groups and an acidic character, which resulted from chemical activation by H_3PO_4. An iodine index of 824.85 mg g^{-1} was achieved for optimal preparation. Crystal violet adsorption studies show a pseudo-first-order kinetic process and fit well with the Freundlich isotherm model, and thus, the predicted adsorption capacity was 364.27 mg g^{-1}.

Received 4th October 2022
Accepted 11th November 2022

DOI: 10.1039/d2ra06220h

rsc.li/rsc-advances

1 Introduction

Since antiquity, activated carbon (AC) has been prepared from any solid material loaded with carbon.[1] It is a material known for its porous structure, thermostability, and especially for its adsorbent characteristic.[2] It is increasingly used in the separation and purification processes of fluid effluents; it is also applied as a support for catalysts, supercapacitors, electrodes, and gas storage processes.[3–5]

The control of its texture, porosity, and chemical characteristics requires the control and optimization of parameters that influence its production process by physical and/or chemical activation.[6,7] Typically, the physical activation consists of the pyrolysis of the precursor material and the activation of the resulting char in steam or carbon dioxide. Chemical activation is a single-step process and is held in the presence of a chemical activator, such as KOH, NaOH, K_2CO_3, H_3PO_4, and H_2SO_4.[8–11] Physical activation under atmospheric vacuum is slightly reported by literature and presents several advantages such as a shorter residence time of volatile matter, a more oxidant-sensitive biochar surface, and high carbon yield.[12,13] Therefore, it is expected that activated carbon has important properties.[13,14] This is attributed to the effect of the vacuum condition that reduces oxygen in the system, limits the secondary reaction of the dangerous organic vapor, and avoids environmental pollution by recovering these gases. Recently, the use of lignocellulosic wastes as a precursor for the production of activated carbon has increasingly attracted scientists,[15,16] such as almond shells that account for about 50% of almond production and is characterized by a high content of lignocellulosic materials and a spongy structure because of their high volatile content, high fixed carbon content, low ash content, zero sulfur content, and low nitrogen content, making it a competitive alternative precursor for the preparation of activated carbon, as well as its availability and low

[a]*Signals, Systems and Components Laboratory (SSCL), Faculty of Sciences and Techniques, Sidi Mohammed Ben Abdellah University, Road Imouzzer BP 2202, Atlas, Fez, Morocco. E-mail: Hamza.boulika@usmba.ac.ma*

[b]*Processes, Materials and Environment Laboratory (PMEL), Faculty of Sciences and Techniques, Sidi Mohammed Ben Abdellah University, Road Imouzzer, BP 2202, Atlas, Fez, Morocco*

cost compared to conventionally used raw materials, which are expensive and non-renewable.[17]

Experimental design methodology (EDM) has become a method of choice for assessing factors. A preliminary study using the asymmetric screening design (ASD) of the parameters influencing the preparation of activated carbon was achieved. This type of plan is required to obtain preliminary information on the influence of these variables on the quality of activated carbon.[18] They can generally indicate the trend of the obtained response at various levels of the factors and give indications of the choice of the experimental field to be studied in the final optimization stage.[19] The important selected factors have been optimized by the response surface methodology based on the central composite design to determine the optimal operating conditions of the system.

In this context, this study contributes to the protection of the environment by developing activated carbons based on almond shells *via* an eco-compatible method involving chemical preparation and physical preparation *via* pyrolysis under vacuum. The optimization of the various factors influencing the preparation of the activated carbon by experimental design methodology was achieved. The characterization of the final product made it possible to prove its thermal stability, morphology, and determine its crystallinity, functional groups, surface functions, and pH with zero charges. The adsorption of a cationic dye, namely, crystal violet, onto the optimal activated carbon, was conducted.

2 Results and discussion

2.1 Statistical validation of the model

The statistical validation of the proposed model in the preliminary study concerning the most influencing factors on the preparation of activated carbon by factorial screening design was based on three main criteria–analysis of variance (ANOVA), coefficients of determination (R^2 & R^2 adjusted), and residue analysis.[25,33]

The results showed that the main effect of the regression is significant since the probability of significance of the *p*-value risk is 0.0524, which is less than 0.1 for 90% confidence level (Table 1). In addition, the model does not show a lack of fit. The calculated values of the R^2 coefficients of determination and the adjusted R^2 are 98% and 95%, respectively, and are sufficient to validate the model since these letters give good agreement between the experimental and predicted values.

The results of standardized residual distribution (Fig. 1A) are consistent with those obtained by the analysis of the variance

Table 1 Analysis of variance for the screening section

Source variation	Sum squares	Freedom degree	Medium square	Ratio	*p*-value
Regression	5.2803×10^4	10	5.2803×10^3	35.1783	0.524
Residual	7.5051×10^2	5	1.5010×10^2		
Sum	5.3553×10^4	10			

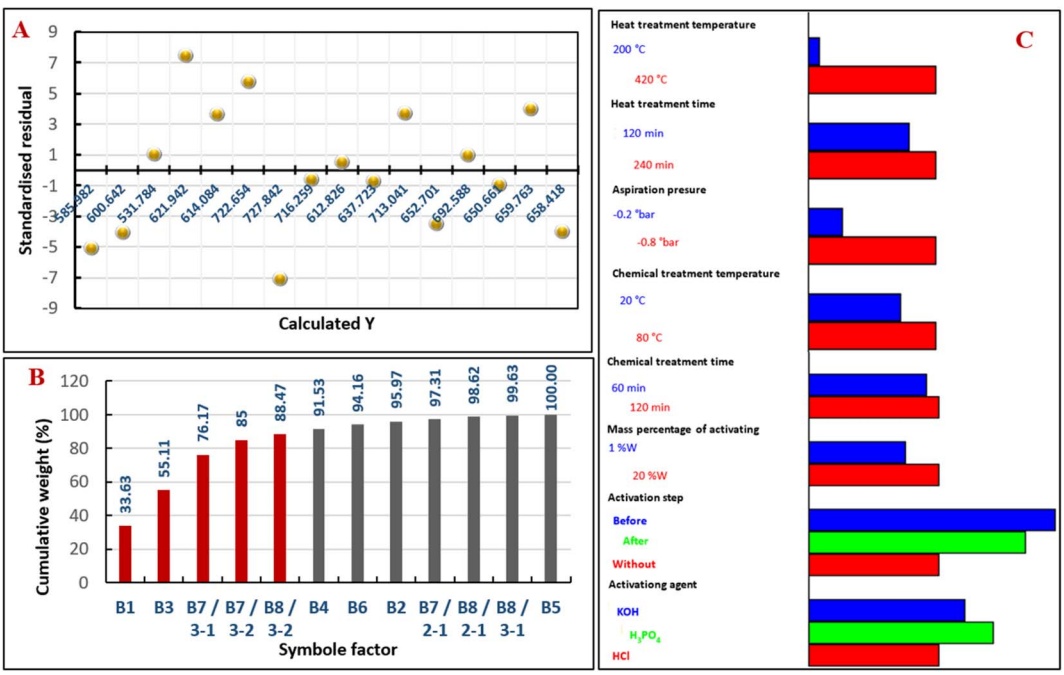

Fig. 1 Standardized residual distribution graph (A), Pareto chart of the cumulative weight contribution (B), graphical study of the level factors influencing the direction (C).

cited in Table 1; they show that the residues are distributed randomly as a function of the response Y. Based on these results, we conclude that the appropriate model is well validated.

2.2 Study of the effects of the main factors

The results of the experimental design are presented in the form of a histogram (Fig. 1B). The analysis of the Pareto diagram, representing the weight of the cumulative contribution of each factor to the construction of the proposed model, reveals that 88% (red color of the histogram bar) of this contribution results from the heat physical treatment temperature (B1), vacuum pressure (B3), chemical activation before the physical treatment (B7), and chemical activation using phosphoric acid (B8). This means that the other factors have no significant effect on iodine index response; therefore, they do not influence the preparation of activated carbon. The direction of the response variation as a function of the level factor and their contribution weights made it possible to construct the histogram of factors and their direction of influence, as shown in Fig. 1C. It is noted that all quantitative factors have a positive effect with different contribution weights, while qualitative factors have important effects on chemical activation by phosphoric acid before physical treatment; this is in agreement with the results previously published.[34–36]

The temperature of the heat treatment has a significant effect on the preparation of activated carbon since the increase in this latter leads to the development of pores; therefore, the structure becomes more porous due to the degradation of volatile organic compounds,[37] which makes it possible to achieve a high iodine index. The suction of the gases formed during the heat treatment promotes the kinetics of formation of the developed activated carbon and makes it possible to avoid the fixation of these gases on the walls of the pores; consequently, the porosity is in direct relation with this factor. The chemical activation of activated carbon before physical treatment facilitates carbonization and develops more structural properties by creating significant porosities in carbon.[38] This is due to the removal of much of the volatile organic matter. The reaction of H_3PO_4 with the biopolymers (lignins, hemicelluloses, and cellulose) results in the formation of biopolymer fragments crosslinked by phosphate and polyphosphate bridges,[39] which accelerates their thermal degradation and leads to high porosity.

2.3 Composite design optimization

The optimization of the temperature of the heat treatment (B1) and the suction pressure (B3) (most influential quantitative factors) on the response was carried out using a central composite design with three central test points, keeping the same level as the previous study factors (Table 2).

2.3.1 Model validation. The statistical significance of the quadratic model equation was evaluated by analysis of variance (ANOVA) and a Fisher test, showing that the regression was statistically significant at 95%. The variance due to regression is much greater than the residual variance (ANOVA 1; p-value = 0.01 < 0.05), which means that there is a link between the factors chosen and the response. There is no significant difference between the variance of lack of fit and the variance of a pure experimental error (ANOVA 2; p-value = 1.68 > 0.05) (Table 3). The model has a coefficient of determination R^2 of 0.98 and an adjusted coefficient of determination ${R_{ajd}}^2$ of 0.96. The closer the model is to the experimental data, the smaller the difference between these data and the predicted values. The distribution of residues according to the response is random (Fig. 2), which confirms that there is no link between the sources of variation.[40] Based on the results of coefficient estimation and the study of the interactions between the various factors governing the iodine index response, the mathematical model representing the Y response as a function of the most influential factors is expressed by eqn (1).

$$Y = 565.705 + 114.21x_1 + 32.78x_2 + 108.53{x_1}^2 + 10.19{x_2}^2 + 7.93x_1x_2 \quad (1)$$

2.3.2 Optimization by response surface methodology. To study the effects of the two selected factors (heat treatment

Table 2 Summarizes the experimental areas of factors with the new ratings

Factor	Designation	Central level (0)	Step variation
Heat treatment temperature (°C)	X_1	310	110
Vacuum pressure (bar)	X_2	−0.5	−0.3

Table 3 Analysis of variance for the optimization section

Source variation	Sum squares	Freedom degree	Medium square	Ratio	p-value
Regression	1.18982×10^5	5	2.37964×10^4	1776.045	<0.01
Residual	2.38303×10^3	5	4.76605×10^2		
Lack of fit	2.35623×10^3	3	7.85410×10^2	58.6191	1.68
Pure experimental error	2.6797	2	13.3985		
Sum	1.21365×10^5	10			

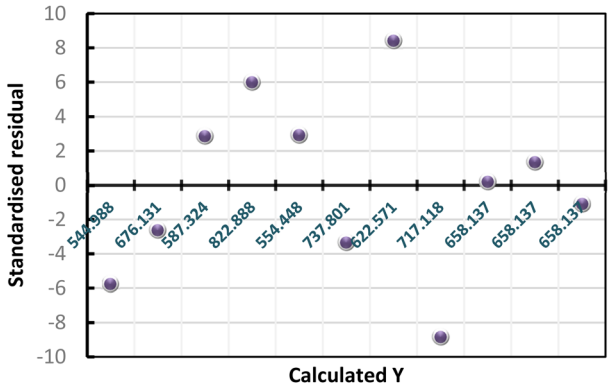

Fig. 2 Standardized residual distribution graph for the optimization section.

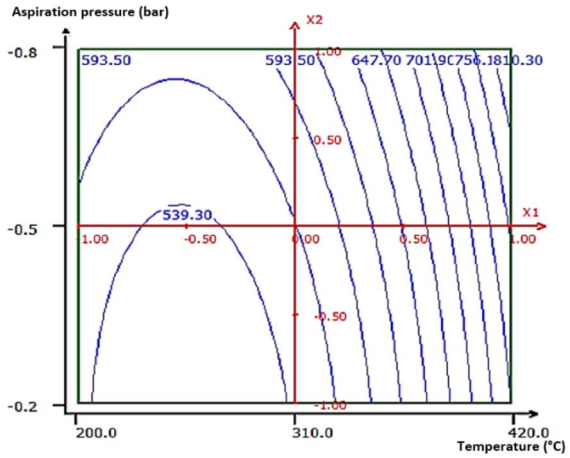

Fig. 3 Level arcs and response surface showing the effect of heat treatment temperature (X_1) and suction pressure (X_2).

temperature and suction pressure) on the iodine index, surface and response methodology were applied; the contour plots are shown in Fig. 3. The predicted maximum surface area is indicated by the surface confined in the highest arc of the contour diagram, the optimum point for the surface (Y) indicated by the model corresponds to 420 °C for the heat treatment temperature with a suction pressure of −0.8 bar to reach an iodine index of 824.85 mg g^{-1}.

2.4 Optimally-activated carbon characterization

2.4.1 Scanning electron microscopy-coupled EDX. The scanning electron microscopic (SEM) observation of the developed powdered activated carbon shows a heterogeneous and coarse texture with an irregular and highly porous surface and a pore diameter of about 10 μm (Fig. 4A and B) that could suggest the presence of mesopores randomly distributed in the macroporous walls (Fig. 4C).

The results of the qualitative analysis obtained by SEM assisted by an electronic microprobe (EDX) (Fig. 4D) reveal the dominant presence of carbon with a small percentage of oxygen and traces of phosphorus. This suggests that this material consists essentially of graphite carbon; the presence of phosphorus is due to activation by phosphoric acid, which has reacted with the acidic surface functions.

2.4.2 Fourier transform infrared spectroscopy. The analysis of the infrared absorption spectrum (FT-IR) of carbon produced under optimum conditions (Fig. 5A) indicated the presence of functional groups due to the chemical treatment of the material. The absorption bands at about 2260 cm^{-1} and 2100 cm^{-1} are characteristics of the groups corresponding to the C≡C alkynes,[41,42] and the band at 1580 cm^{-1} is related to the stretching of the C=C bonds of the olefins (alkenes) and of the benzyl rings.[43] A wide band at about 1100 cm^{-1} corresponding to the deformation in the plane of the C–O aliphatic bonds is attributed to the carboxylic acids.[44] The phosphonate groups exhibiting the characteristic absorption band at about 1055 cm^{-1} is attributed to the stretching of the P–OH bond.[45] The bands at about 990 cm^{-1} and 750 cm^{-1} are linked to the vibrations of the C–H bond.[34,35]

2.4.3 X-ray diffraction. The diffractogram of the prepared activated carbon has a wide peak in the 2θ range of 20° to 25° and another less intense diffraction peak spread between 40° and 45° (Fig. 5B), which are attributed to amorphous carbon.[4,36] These two large diffraction peaks are generally attributed to the graphite crystal planes of the activated carbon in the low angle region ((002) of the graphite peak) and the radial spread of the crystal structures in the high angle region ((100) of the graphite peak).[2] Consequently, the obtained activated carbon is in the form of disorganized graphite.

2.4.4 Thermogravimetric analysis. The analysis of the data from the TG and its first derivative (DTG) of the optimal activated carbon is noted in Fig. 5C, which shows a first mass loss of about 14% when the sample is heated to 140 °C due to the evaporation of trapped water in the pores of the activated carbon. Notable thermal stability is observed between 140 °C and 360 °C. A second continuous mass loss noted from 360 °C to 480 °C is related to the decomposition of the fragments of the crosslinked acid functions by phosphate and polyphosphate bridges formed during the chemical activation. A third mass loss of 38% is revealed between 510 °C and 550 °C, expressed as an intense differential peak at about 510 °C related to the total degradation of the activated carbon.

2.4.5 Zero charge pH. The monitoring of the acid-base behavior makes it possible to plot the curve of the pH of zero charges of the activated carbon (Fig. 5D). The obtained pH_{pzc} is 4.5; the adsorbent surface is charged positively at a pH lower than 4.5 and negatively at a pH higher than 4.5. When the pH tends toward the pH of zero charges, the density of negatively charged ions on the carbon surface increases.

2.4.6 Acid-base groups of surfaces. The results of the identification and quantification of the oxygenated groups on the surface of the material produced using Boehm titration are detailed in Table 4. They showed that the material produced was characterized by an acidic surface with a concentration of 1.699 meq g^{-1}; however, a presence of 0.52 meq g^{-1} of basic functional groups was noted.

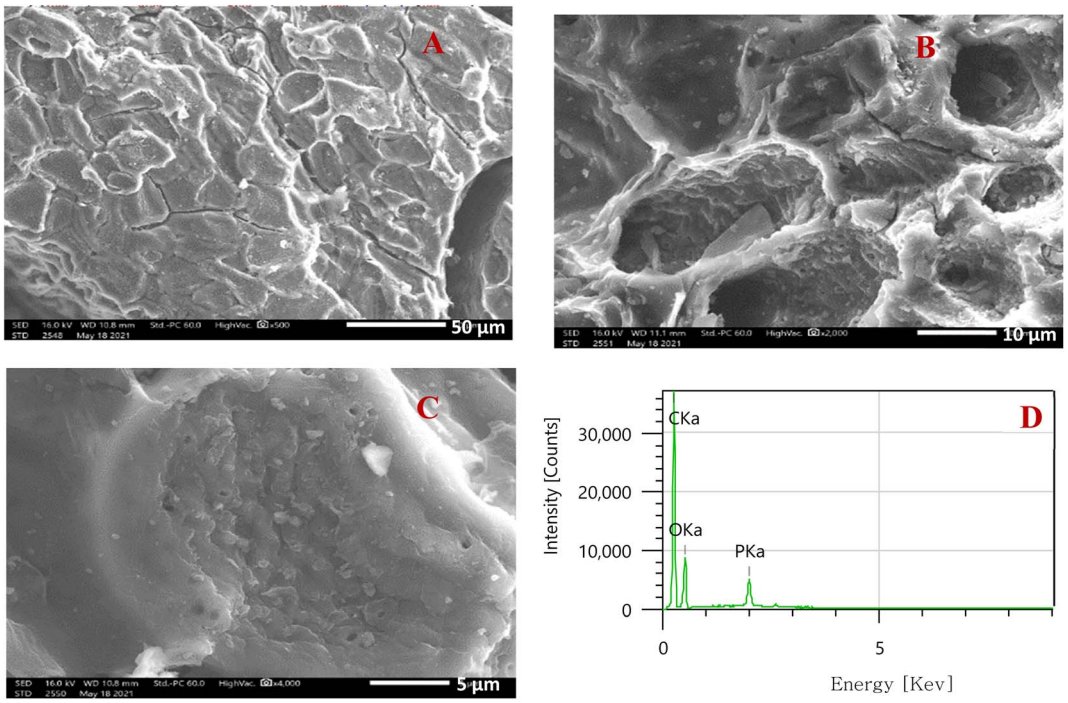

Fig. 4 Microphotographs of activated carbon produced at various enlargements: ×500 (A), ×2000 (B), ×4000 (C), and EDX analysis (D).

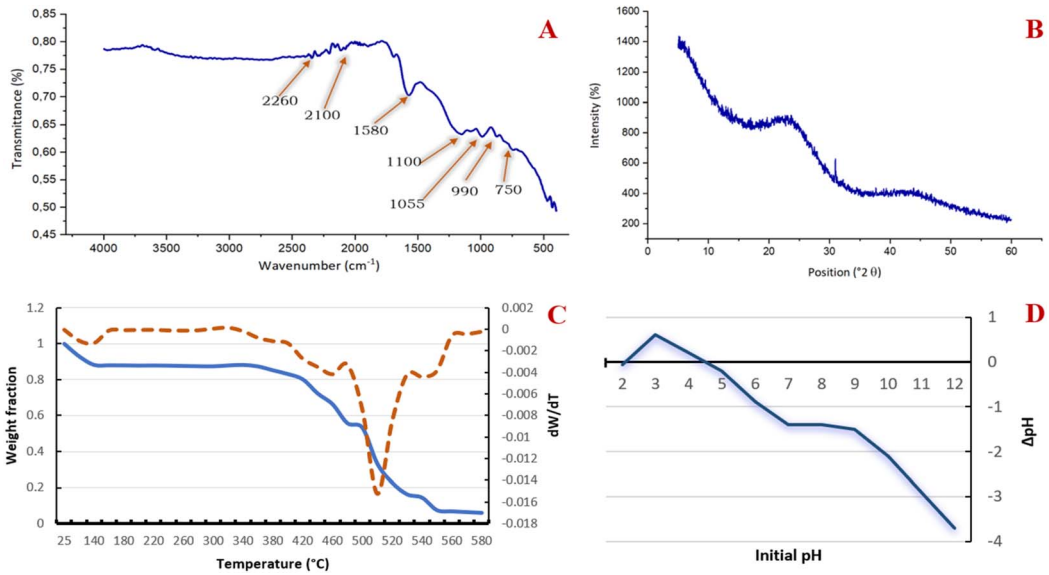

Fig. 5 Optimally prepared activated carbon characterization analysis: FT-IR spectrum (A), X-ray diffractogram (B), TG and DTG curves (C), pH determination curve at zero charge (D).

2.5 Crystal violet (CV) adsorption on the optimal activated carbon

The effect of pH on CV adsorption over a range of 3 to 6 as a function of time was studied (Fig. 6A). The obtained results showed that the maximum adsorption was observed at pH = 5 after 20 min. The pH_{pzc} being 4.5, the surface of the activated carbon produced under the optimum experimental conditions is therefore negatively charged, which leads to electrostatic attractions between the positively charged CV molecules and the pore surface of the negatively charged activated carbon.[49,50] This improves the fixation of the dye molecules into the activated carbon surface. At pH = 3, the adsorption equilibrium was not clearly achieved and presents the lowest removal rate as H^+ protons compete with positively charged dye molecules by binding to the surface of the carbon.[49]

Table 4 Concentration of surface groups of activated carbon determined by the Boehm method

Oxygen functions	Concentration (meq g^{-1})
Strong carboxylic acid	0.94
Lactone and weak carboxylic acid	0.089
Hydroxyl and phenol	0.67
Total acid functions	1.699
Basic functions	0.52

The obtained results indicate a maximum adsorption percentage of 91.77% after 30 min of contact for 10 ppm CV concentration (Fig. 6B). The observed decrease could be explained by the saturation of the active pores due to the high concentration of the dye toward the available adsorption sites. These results are in agreement with several previous works.[51–54,58]

2.5.1 Kinetic and isothermal adsorption studies. To identify the kinetic model and the mechanisms of the adsorption kinetics of CV on AC, two models were used. The modeling curves are shown in Fig. 7 and 8. The linearity study of the experimental data and those predicted for the models, and the value analysis of the kinetic constants, isothermal adsorption parameters, adjusted coefficient of determination ($R_{ajd}^2 > 0.99$), and the lowest standard deviation between the experimental and calculated values and probability value in Tables 5 and 6 shows better agreement with the pseudo-

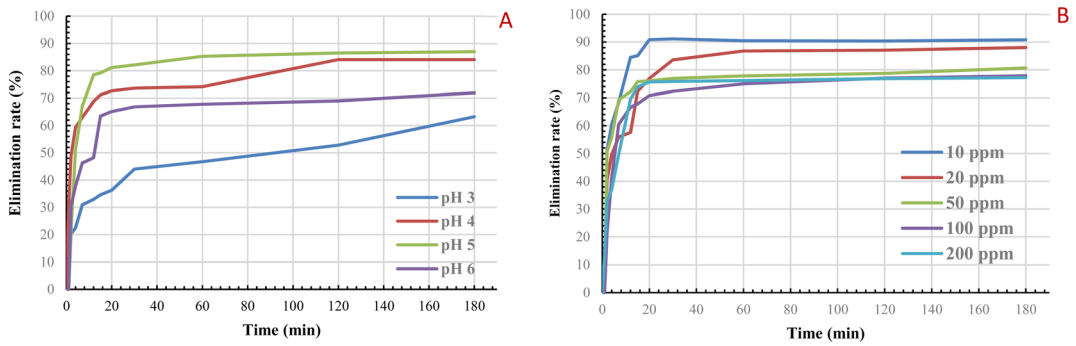

Fig. 6 Evolution of the elimination rate as a function of contact times at different pH values (T = 25 °C, m (AC) = 1 g, [CV] = 100 ppm) (A), evolution in the adsorption rate as a function of contact times at different initial concentrations of the dye (T = 25 °C, m (AC) = 1 g, pH = 5) (B).

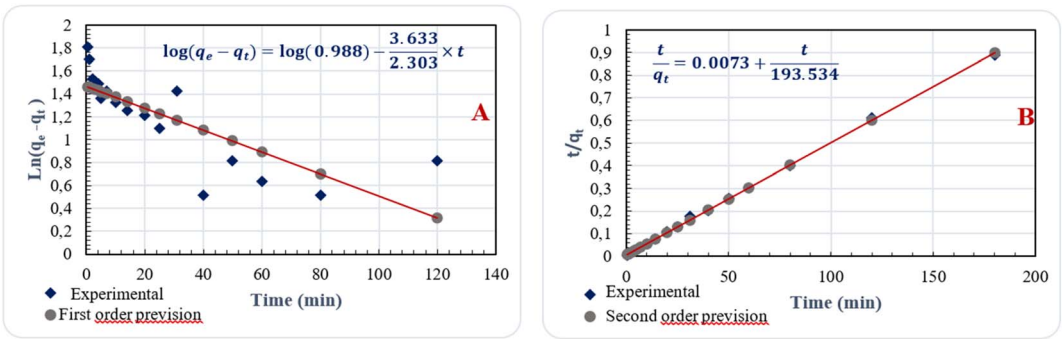

Fig. 7 Curves illustrating the kinetic model of adsorption on AC; pseudo-first order (A), pseudo-second order (B), DC = 100 ppm (MG), pH = 5 for (MG), T = 25 °C.

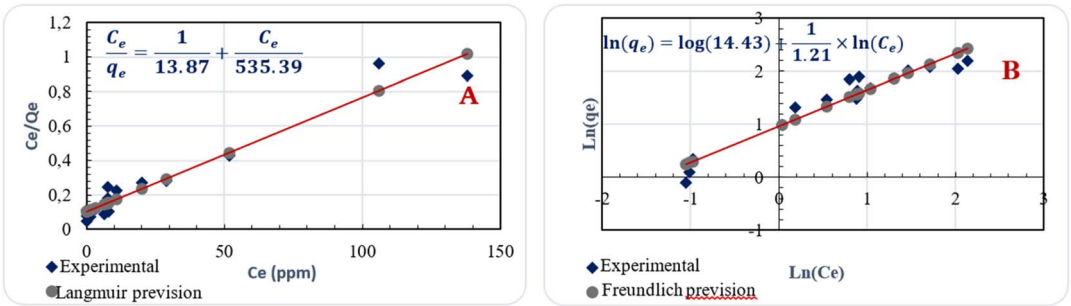

Fig. 8 Modeling of adsorption isotherms of CV on AC; langmuir (A) and freundlich (B).

Table 5 Parameters and their validity criteria of the pseudo-first-order and pseudo-second-order model for the adsorption of CV on CA

Kinetic model	Parameter	Value	Adjusted correlation coefficient	Standard deviation	*p*-value
Pseudo-first order	Q_e (mg g^{-1})	**0.9888**	0.6579	0.2790	0.0002
	K_f (min^{-1})	**−3.6333**			
Pseudo-second order	Q_e (mg g^{-1})	**193.5341**	0.9994	0.0062	0.0000
	K_f (min^{-1})	**0.0036**			

Table 6 Parameters of the different isothermal models for the study of the adsorption of CV on CA at 298 K

Isothermal models	Parameter	Value	Adjusted correlation coefficient	Standard deviation	*p*-value
Langmuir	Q_m (mg g^{-1})	**535.99**	0.4518	0.0310	0.0043
	K_l (L mg^{-1})	**0.03**			
Freundlich	$1/n$	**0.83**	0.9660	0.1527	1.1031×10^{11}
	K_f (mg g^{-1})	**14.43**			

second-order kinetic model, and thus well describes the adsorption phenomenon through the establishment of chemical bonds (interactions) between the adsorbates and the functional groups on the surface of the adsorbents that are responsible for the adsorption capacity of the adsorbents.[55,56] The Freundlich isotherm adsorption model fits the phenomenon well, and the predicted adsorption capacity by the validated isotherm model is 364.27 mg g^{-1}. These results are competitive with recent research reported on the adsorption of CV onto activated carbon prepared from the rubber seed pericarp;[57] Rafiee *et al.* 2020 prepared activated carbon from a pistachio shell for the adsorption of a CV, whose maximum adsorption capacity reached 196.08 mg g^{-1}.[46]

Table 7 compares the present preparation method with other methods of activated carbon from almond shells by the iodine index as a basic characteristic for the porosity of activated carbon and the adsorption efficiency toward the organic pollutants. The highest activated carbon iodine index (824.85 mg g^{-1}) and the elimination of organic pollutants are achieved by the present method. The other methods are complex and not eco-compatible compared to this work. Thus, the prepared activated carbon has good properties as a low-cost adsorbent for water remediation.

Table 7 Comparison study of activated carbon from almond shell by several processes

Almond shell origin	Preparation method	Iodine index (mg g^{-1})	Adsorption efficiency	Reference
The northern region of Morocco	Chemical activation phosphoric acid (1% W) activation agent before a physical treatment at 420 °C under vacuum (−0.8 bar)	824.85	364.27 mg g^{-1} for crystal violet dye	This study
Turkey	Chemical activation phosphoric acid activation agent before applying both conventional heating (500 °C) and microwave heating (500 W) in succession	791	148 mg g^{-1} for methyl blue dye	İzgi *et al.* 2018 (ref. 47)
Turkey	Chemical activation by a solution of $ZnCl_2$ (30 wt%) and a carbonization at 850 °C under N_2 flow (40 mL min^{-1})	638	1.33 mg g^{-1} for methyl blue dye	Aygün *et al.* 2003 (ref. 49)
Iran	Microwave-assisted impregnation	812	—	Teimouri *et al.* 2019 (ref. 61)
Tunisia	Carbonization under carbon dioxide flow of 100 cm^3 min^{-1} at 800 °C with chemical modification using NH_3	414.78	78%	Omri *et al.* 2013 (ref. 48)

3 Materials and methods

3.1 Materials

Almond shells were collected from an industrial unit in the Fez region of Morocco, separated manually from their hull, washed, dried at 60 °C for 24 h, then crushed and sieved. A fraction between 3.15 and 1.25 mm in diameter was selected to be used in the production of activated carbon. Table 8 summarizes the physicochemical characteristics of the used almond shells.

3.2 Methods

3.2.1 Preparation of activated carbon process. 1 g of the pre-treated sample was impregnated with stirring in 5 mL of an aqueous solution of activating agent (1 g: 5 mL), then filtered under vacuum, and the filtrate was washed with distilled water until a neutral pH was obtained. The activated sample was dried at 110 °C for 12 h and then subjected to a physical treatment using a system developed in the laboratory allowing carbonization under vacuum with the recovery of the resulting polluted gases by trapping them in distilled water.

3.2.2 Experimental design methodology. For any process, it is important to know the influence of different physicochemical parameters (control factors) on the results of the process. Asymmetric Screening Design (ASD) was used to reduce the number of total experiments to identify those that influence the process of preparing activated carbon.[20] We studied the effect of eight essential parameters and six quantitative factors at two levels: the treatment temperature, heat treatment time, suction pressure, chemical activation time, chemical activation temperature, and chemical activator percentage. The other two qualitative factors at three levels are the chemical activator type and the chemical activation step, which leads to a matrix of sixteen experiments. The response chosen is the iodine index, which makes it possible to determine the porosity of the activated carbon and evaluate its quality.[21] Factor levels were selected based on preliminary experiences and previous works (Table 9).[22–24]

Table 8 Physicochemical characteristics of almond shell raw material

Characteristics	Value
Moisture (% wt)	8.82 ± 0.74
Volatile matter (% wt)	73.08 ± 0.66
Ash (% wt)	2.55 ± 0.21
Fixed carbon (% wt)	15.55 ± 0.44
Extractives (% wt)	12.64 ± 0.52
Lignin (% wt)	27.51 ± 0.58
Hemicellulose (% wt)	26.73 ± 1.38
Cellulose (% wt)	30.94 ± 0.23

Table 9 Screening parameters and study levels

		Levels		
Factor	Designation	1	2	3
Heat treatment temperature (°C)	B1	200	420	
Heat treatment time (min)	B2	120	240	
Suction pressure (bar)	B3	−0.2	−0.8	
Chemical treatment time (min)	B4	60	180	
Chemical treatment temperature (°C)	B5	20	80	
Chemical activator percentage (%)	B6	5	20	
Chemical activation step	B7	Before	After	Without
Chemical activator type	B8	KOH	H_3PO_4	HCl

Response surface methodology allows the defining of the optimal experimental conditions to achieve a maximum adsorption rate (high iodine index). The chosen design is a central composite with k factors, which comprises N_f tests of a complete factorial design $2k$, NA star tests on the axes, and N_0 central tests.[25]

The regression (eqn (2)) is expressed by the second order polynomial model:

$$Y = b_0 + \sum_i b_i x_i + \sum_i b_{ii} {x_i}^2 + \sum_{i \neq j} b_{ij} x_{ij} \quad (2)$$

where Y is the predicted response (adsorption rate), x_i is the independent variables, x_{ij} is the interaction between factors i and j, b_0 is the model constant, b_i is the linear coefficient, b_{ii} are the quadratic coefficients, and b_{ij} is the cross-product coefficients. All analyses and calculations (regression, statistical tests, and graphs) were achieved with Nemrodw software.

The iodine index, expressed in mg g^{-1}, is the amount of iodine (in mg) adsorbed by 1 g of the activated carbon in a 0.02 N aqueous solution of I_2. This index describes the accessibility of any particle of size less than or equal to that of the molecule I_2. Its determination was carried out according to the CEFIC 1989 method and AWWA B604-76 standard.[21]

0.2 g of powdered prepared activated carbon was dispersed in 20 mL of a solution of I_2 (0.02 N). The mixture was stirred for 4 to 5 min, filtered, and then examined with a 0.1 N sodium thiosulfate solution ($Na_2S_2O_3$). The iodine index Q_{I_2} was calculated using the following eqn (3)

$$Q_{I_2} = \frac{C_0 \times C_{th} \times V_{th}}{2 \times V_{I_2}} \times \frac{M_{I_2} \times V_{ads}}{m_{CA}} \quad (3)$$

where C_0 is the initial concentration of I_2, C_{th} is the concentration of $Na_2S_2O_3$, V_{th} is the volume of $Na_2S_2O_3$ at equilibrium, V_{I2} is the volume of I_2 dosed, M_{I2} is the molar mass of I_2, V_{ads} is the I_2 volume, and m_{CA} is the activated carbon mass.

3.2.3 Characterization of activated carbon based on optimal conditions. A JEOL scanning electron microscope, model it500 HR, was used to observe the morphology of the sample surfaces. A Panalytical X'Pert Pro X-ray diffractometer with a Cu-Kα anode of monochromatic source (1.54 Å), set to an operating voltage of 40 kV and a filament current of 30 mA, was used to determine the crystallinity of the sample. The diffractograms were recorded between 2θ values of 5.0044° and 60.1834° with a step of 0.0170°. Thermogravimetric analysis (TGA) of the samples was done using a Q500 thermal analysis instrument over the range from 25 °C to 600 °C with

a heating rate of 5 °C min^{-1}. Fourier Transform Infrared (FT-IR) spectroscopic analysis was carried out by a Bruker Vertex 70 FTIR Spectrophotometer. The main functional groups contained in the sample were determined from the spectra recorded as transmittance in a range from 400 to 4500 cm^{-1}. The pH of zero charges (pH_{pzc}) was measured by dispersing 0.15 g of the activated carbon in 50 mL of a solution of sodium chloride (0.01 M), the pH of each dispersion was adjusted (from 2 to 12, with a step of 1) by adding sodium hydroxide or hydrochloric as appropriate. Stirring was maintained for 48 h using a multi-stirring system at a temperature of 25 °C. The mixtures contents were then filtered using filter paper (pore diameter 0.45 μm).[26] The nature of the surface functional groups was determined according to the Boehm method, which consists of introducing 0.5 g of activated carbon in different double-walled reactors containing 50 mL of separate solutions of HCl (0.1 N), $NaHCO_3$ (0.1 N), Na_2CO_3 (0.1 N), and NaOH (0.1 N). The mixtures were stirred magnetically at 300 rpm for 48 h at 20 ± 2 °C. After filtration, the excess of the base or acid was titrated respectively by a solution of HCl (0.05 N) or NaOH (0.05 N).[27]

3.2.4 Adsorption test of crystal violet on activated carbon. The optimal activated carbon was dried for 4 h in an oven at a temperature of 140 °C and then cooled in a desiccator. For the batch adsorption experiments, 1 g of the activated carbon was dispersed in one liter of a solution of Crystal Violet (CV) ($C_{25}H_{30}N_3Cl$). The mixture was stirred at 250 rpm at 25 °C for various contact times of up to 120 min. A preliminary study of the pH effect on the adsorption rate was investigated by varying the pH from 2 to 6 using a hydrochloric acid solution. Different concentrations of CV solutions (10–200 mg L^{-1}) were selected to study the effect of the dye concentration on the adsorption rate. Aliquots were taken from the reaction mixture at different time intervals; the remaining dye concentrations were determined using a UV/visible spectrophotometer at a maximum wavelength of 582 nm.

The adsorption capacity q_e (mg g^{-1}) and percent removal (% R) of the dye were calculated using eqn (4) and (5)

$$q_e = \frac{C_0 - C_e}{m} \times V \quad (4)$$

$$\%\ R = \frac{C_0 - C_e}{C_0} \times 100 \quad (5)$$

where C_0 and C_e are the initial and equilibrium dye concentrations (mg L^{-1}), respectively, V is the dye solution volume (L), and is m the mass of the adsorbent (g).

3.2.4.1 Kinetic models of adsorption. The kinetics of adsorption was studied using two models, namely, pseudo-first-order[28] and pseudo-second order.[29] The conformity of the experimental data with the predicted values by the applied models was expressed by the fitted correlation coefficients (R_{ajd}^2) and the probability value (p_{value}).

• The pseudo-first order model is expressed by eqn (6)

$$\log(q_e - q_t) = \log(q_e) - \frac{K_f}{2.303} \times t \quad (6)$$

where k_f is the pseudo-first order kinetic constant (min^{-1}), q_t and q_e are the adsorption capacities (mg g^{-1}) at time t and at equilibrium, respectively, and t is the contact time (min).

• The pseudo-second order model is expressed by eqn (7)

$$\frac{t}{q_t} = \frac{1}{K_s \times q_e^2} + \frac{t}{q_e} \quad (7)$$

where k_s is the pseudo-first order kinetic constant (g mg^{-1} min^{-1}), q_t and q_e are the adsorption capacities (mg g^{-1}) at time t and equilibrium, respectively, and t is the contact time (min).

3.2.4.2 Modeling of adsorption isotherms. The adsorption isotherm is used to describe the equilibrium distribution of the dye between the solid and liquid phases at a given temperature when equilibrium is reached. Langmuir and Freundlich isotherms were applied to fit the equilibrium data 9. Each isotherm is expressed by relative constants that characterize the surface properties and indicate the adsorption capacity of the material.[30]

3.2.4.2.1 Langmuir isotherm. Langmuir isotherm model assumes that the adsorption is monolayer and occurs at the surface of the solid with identical homogeneous sites.[31] It also suggests that no further adsorption takes place once the active sites are covered with dye molecules. The saturated Langmuir isotherm is represented by eqn (9)[59]

$$\frac{C_e}{q_e} = \frac{1}{q_m \times K_L} + \frac{C_e}{q_t} \quad (8)$$

where C_e is the equilibrium concentration (mg L^{-1}), q_t and q_e are the adsorption capacities (mg g^{-1}) at time t and equilibrium, respectively, q_m is the theoretical maximum adsorption capacity (mg g^{-1}), and K_L is a constant denoting the adsorption energy and the affinity of the binding sites (L mg^{-1}).

3.2.4.2.2 Freundlich isotherm. The Freundlich isotherm is an empirical model assuming that the thermal distribution on the surface of the adsorbent is non-uniform, corresponding to heterogeneous adsorption.[32] It is expressed by eqn (9)

$$\log(q_e) = \log(K_f) + \frac{1}{n_f} \times \log(C_e) \quad (9)$$

where C_e is the equilibrium concentration (mg L^{-1}), q_e is the adsorption capacity (mg g^{-1}) at equilibrium, n_f and K_f (mg g^{-1}) are the two Freundlich constants giving an indication of the adsorption intensity and capacity, respectively.[60]

4 Conclusion

The use of the almond shells as a precursor for the production of activated carbon by chemical activation using H_3PO_4 before physical treatment under vacuum is an eco-compatible method, where the aspired gases are condensed in distilled water to prevent their release into the environment. Their optimization by the experimental design methodology was carried out. The screening of eight parameters to test their influence on the developed process made it possible to select four factors that have a very significant influence on the quality of the activated

carbon prepared. The optimization of these factors was carried out by fixing two qualitative factors in their optimum, namely, the chemical activation with H_3PO_4 before the physical treatment and by varying the two quantitative factors by a central composite design. A physical treatment temperature of 420 °C and a vacuum pressure of −0.8 bar were adopted and led to a maximum iodine value of about 824.85 mg g^{-1}. Infrared spectroscopy reveals the presence of acid and phosphonates groups due to activation by H_3PO_4. X-ray diffraction shows a disorganized graphical structure, thermogravimetric analysis indicates significant thermal stability between 140 °C and 360 °C, scanning electron microscopy coupled to the EDX reveals an irregular and porous outer surface as well as the presence of carbon and oxygen and traces of phosphorus. The surface groups determined by the Boehm method are acidic with a pH_{pzc} of 4.5. These characteristics are important indications of the effectiveness of this newly developed method. The kinetic and isotherm adsorption studies of crystal violet on the optimal activated carbon fits the pseudo-first-order model and the Freundlich isotherm model; thus, the predicted adsorption capacity is 364.27 mg g^{-1} at a pH of 5.

Data availability

The datasets used and/or analyzed during the current study are available from the corresponding author upon reasonable request.

Author contributionsHamza Boulika: conceptualization, visualization, data curation, investigation, methodology, writing – original draft preparation. Maryam El Hajam: visualization, writing—review & editing. Meryem Hajji Nabih: data curation, investigation. Noureddine Idrissi Kandri: conceptualization, formal analysis, methodology, data curation. Aziz Zaroual: writing – reviewing and editing, validation.

Conflicts of interest

The authors declare that they have no conflict of interest.

References

1 O. Ioannidou and A. Zabaniotou, *Renewable Sustainable Energy Rev.*, 2007, **11**, 1966–2005.
2 J. Zhao, L. Yang, F. Li, R. Yu and C. Jin, *Carbon*, 2009, **47**, 744–751.
3 I. Martin-Gullon, J. P. Marco-Lozar, D. Cazorla-Amorós and A. Linares-Solano, *Carbon*, 2004, **42**, 1339–1343.
4 Y. Chen, Y. Zhu, Z. Wang, Y. Li, L. Wang, L. Ding, X. Gao, Y. Ma and Y. Guo, *Adv. Colloid Interface Sci.*, 2011, **163**, 39–52.
5 J. Bedia, J. M. Rosas, D. Vera, J. Rodríguez-Mirasol and T. Cordero, *Catal. Today*, 2010, **158**, 89–96.
6 S. Yorgun, N. Vural and H. Demiral, *Microporous Mesoporous Mater.*, 2009, **122**, 189–194.
7 K. Li, Z. Zheng and Y. Li, *J. Hazard. Mater.*, 2010, **181**, 440–447.
8 M. Hajji Nabih, M. El Hajam, H. Boulika, Z. Chiki, S. Ben Tahar, N. Idrissi Kandri and A. Zerouale, *Mater. Today: Proc.*, 2022, 1–11.
9 H. Boulika, M. El Hajam, M. Hajji Nabih, I. Riffi Karim, N. Idrissi Kandri and A. Zerouale, *Mater. Today: Proc.*, 2022, DOI: **10.1016/j.matpr.2022.07.358**.
10 M. Molina-Sabio, F. Rodríguez-Reinoso, F. Caturla and M. J. Sellés, *Carbon*, 1996, **34**, 457–462.
11 K. le Van, T. L. T. Thu, H. N. T. Thu and H. van Hoang, *Russ. J. Electrochem.*, 2019, **55**, 900–907.
12 T. Cordero-Lanzac, R. Palos, J. M. Arandes, P. Castaño, J. Rodríguez-Mirasol, T. Cordero and J. Bilbao, *Appl. Catal., B*, 2017, **203**, 389–399.
13 J. Yang and K. Q. Qiu, *Environ. Sci. Technol.*, 2009, **43**, 3385–3390.
14 C. T. Nguyen, D. Tungtakanpoung, V. T. Tra and P. Kajitvichyanukul, *Case Stud. Chem. Environ. Eng.*, 2022, **6**, 100248.
15 M. H. Nabih, M. El Hajam, H. Boulika, M. M. Hassan, N. I. Kandri, A. Hedfi, A. Zerouale and F. Boufahja, *Sustainability*, 2021, 13905.
16 S. Yorgun and D. Yıldız, *J. Taiwan Inst. Chem. Eng.*, 2015, **53**, 122–131.
17 Y. Chen, Y. Zhu, Z. Wang, Y. Li, L. Wang, L. Ding, X. Gao, Y. Ma and Y. Guo, *Adv. Colloid Interface Sci.*, 2011, **163**, 39–52.
18 L. Torbjorn, E. Seifert, L. Abramo, B. Thelin, A. Nystrom, J. Pettersen and R. Bergman, *Handb. Environ. Chem.*, 1995, vol. 2, pp. 73–122.
19 R. W. Mee and J. L. Goupy, *Methods for Experimental Design: Principles and Applications for Physicists and Chemists*, Elsevier B.V., 1995, vol. 90.
20 J. E. Reece, S. N. Deming and S. L. Morgan, *Am Stat*, 1994, **48**, 172.
21 H. Rushing, A. Karl and J. Wisnowski, *Handbook of Reading Research*, 2016, pp. 63–90.
22 M. Molina-Sabio and F. Rodríguez-Reinoso, *Colloids Surf., A*, 2004, **241**, 15–25.
23 J. Xu, L. Chen, H. Qu, Y. Jiao, J. Xie and G. Xing, *Appl. Surf. Sci.*, 2014, **320**, 674–680.
24 C. A. Toles, W. E. Marshall, M. M. Johns, L. H. Wartelle and A. Mcaloon, *Bioresour. Technol.*, 2000, **71**, 87–92.
25 H. Demiral, I. Demiral, F. Tümsek and B. Karabacakoğlu, *Surf. Interface Anal.*, 2008, **40**, 616–619.
26 A. Tyagi, S. Banerjee, S. Singh and K. K. Kar, *Int. J. Hydrogen Energy*, 2019, **45**, 16930–16943.
27 E. Yagmur, M. Ozmak and Z. Aktas, *Fuel*, 2008, **87**, 3278–3285.
28 R. A. Olivero, J. M. Nocerino and S. N. Deming, *Handbook of Environmental Chemistry*, 1995, vol. 2, pp. 73–122.
29 G. Socrates, *Infrared and Raman Characteristic Group Frequencies Tables and Charts*, John Wiley & Sons, New york, 1980, vol. 296.
30 A. S. Politou, C. Morterra and M. J. D. Low, *Carbon*, 1990, **28**, 529–538.
31 M. el Hajam, N. Idrissi Kandri, A. Harrach, A. el khomsi and A. Zerouale, *Mater. Today: Proc.*, 2019, **13**, 803–811.

32 A. S. Politou, C. Morterra and M. J. D. Low, *Carbon*, 1990, **28**, 529–538.
33 A. M. Puziy, O. I. Poddubnaya, A. Martı, J. M. D. Tasco, A. Castro-Mun and F. Sua, *Carbon*, 2007, **45**, 1941–1950.
34 K. Bilba and A. Ouensanga, *J. Anal. Appl. Pyrolysis*, 1996, **38**, 61–73.
35 G. Socrates, *Infrared and Raman Characteristic Group Frequencies Tables and Charts*, John Wiley & Sons, New york, 1980, vol. 296.
36 J. Zhang, Z. Zhong, H. Guo and X. Jiang, Preparation of Bamboo-Based Activated Carbon, *2010 Asia-Pacific Power and Energy Engineering Conference*, 2010, pp. 1–4.
37 R. M. M. dos Santos, R. G. L. Gonçalves, V. R. L. Constantino, C. V. Santilli, P. D. Borges, J. Tronto and F. G. Pinto, *Appl. Clay Sci.*, 2017, **140**, 132–139.
38 M. el Hajam, N. Idrissi Kandri and A. Zerouale, *Moroccan J. Chem.*, 2019, **7**, 431–435.
39 R. Ahmad, *J. Hazard. Mater.*, 2009, **171**, 767–773.
40 A. Mittal, J. Mittal, A. Malviya, D. Kaur and V. K. Gupta, *J. Colloid Interface Sci.*, 2010, **343**, 463–473.
41 Y. C. Sharma, Uma and S. N. Upadhyay, *Can. J. Chem. Eng.*, 2011, **89**, 377–383.
42 M. el Hajam, N. Idrissi Kandri, A. Harrach, A. el khomsi and A. Zerouale, *Mater. Today: Proc.*, 2019, **13**, 812–821.
43 Y. S. Ho, *J. Hazard. Mater.*, 2006, **136**, 681–689.
44 Z. Hussain, R. Kumar and D. Meghavathu, *Int. J. Eng. Technol.*, 2018, **7**, 284–287.
45 M. Kashif Uddin, A. M. Nurul Najwa, A. H. Jawad and S. Sabar, *Int. J. Phytorem.*, 2022, DOI: **10.1080/15226514.2022.2086214**.
46 A. Rafiee, S. Ghanavati Nasab and A. Teimouri, *Int. J. Environ. Anal. Chem.*, 2020, **100**, 1624–1649.
47 M. S. İzgi, C. Saka, O. Baytar, G. Saraçoğlu and Ö. Şahin, *Anal. Lett.*, 2019, **52**, 772–789.
48 A. Omri, M. Benzina and N. Ammar, *J. Ind. Eng. Chem.*, 2013, **19**, 2092–2099.
49 A. Aygün, S. Yenisoy-Karakaş and I. Duman, *Microporous Mesoporous Mater.*, 2003, **66**, 189–195.
50 R. L. Mason, *Statistical Design and Analysis of Experiments With Applications to Engineering and Science Second Edition*, John Wiley & Sons Publication, John Wiley Sons, 2003.
51 Comm Rep, *J.–Am. Water Works Assoc.*, 1974, **66**, 672–681.
52 C. Pechyen, D. Atong, D. Aht-ong and V. Sricharoenchaikul, *J. Solid Mech. Mater. Eng*, 2007, **1**, 498–507.
53 M. Trachi, N. Bourfis, S. Benamara and H. Gougam, *Biotechnol., Agron., Soc. Environ.*, 2014, **18**, 492–502.
54 S. Yorgun and D. Yildiz, *J. Taiwan Inst. Chem. Eng.*, 2015, **53**, 122–131.
55 J. S. Noh and J. A. Schwarz, *J. Colloid Interface Sci.*, 1989, **130**, 157–164.
56 H. P. Boehm, *Carbon*, 1994, **32**, 759–769.
57 Y. S. Ho and G. McKay, *Process Biochem.*, 1999, **34**, 451–465.
58 M. el Hajam, N. I. Kandri, A. Harrach and A. Zerouale, *Stud. Cercet. Stiint.: Chim. Ing. Chim., Biotehnol., Ind. Aliment.*, 2019, **20**, 395–409.
59 I. Langmuir, *J. Am. Chem. Soc.*, 1918, **40**, 1361–1403.
60 H. Freundlich and H. Wilpried, *J. Am. Chem. Soc.*, 1939, **61**, 2228–2230.
61 Z. Teimouri, A. Salema and S. Salem, *J. Environ. Chem. Eng.*, 2019, **7**, 103161.